Coherent X-Ray Raman Spectroscopy: A Nonlinear Local Probe for Electronic Excitations

Satoshi Tanaka[1,3] and Shaul Mukamel[1,2]

[1]*Department of Chemistry, University of Rochester, Rochester New York, 14627*
[2]*Department of Physics and Astronomy, University of Rochester, Rochester New York, 14627*
[3]*College of Integrated Arts and Sciences, Osaka Prefecture University, Sakai 599-8531, Japan*

(Received 27 November 2001; published 9 July 2002)

Nonlinear x-ray four-wave mixing experiments are becoming feasible due to rapid advances in high harmonic generation and synchrotron radiation coherent x-ray sources. By tuning the difference of two x-ray frequencies across the valence excitations, it is possible to probe the entire manifold of molecular electronic excitations. We show that the wave vector and frequency profiles of this x-ray analogue of coherent Raman spectroscopy provide an excellent real-space probe that carries most valuable structural and dynamical information, not available from spontaneous Raman techniques.

DOI: 10.1103/PhysRevLett.89.043001 PACS numbers: 33.20.Rm, 42.65.Dr

Raman spectroscopy uses a difference of two high-frequency fields (ω_1, ω_2) to probe lower frequency resonances $\omega_1 - \omega_2 = \omega_{ab}$. The Raman process is usually performed with optical fields which are resonant with electronic transitions, and the low-frequency Raman resonances correspond to vibrational motions and low-lying electronic excitations. Raman resonances can be observed either through spontaneous Raman scattering (SRS) or coherent Raman scattering (CRS); a third order four-wave mixing process involving three incoming beams $(\mathbf{k}_1, \omega_1)$, $(\mathbf{k}_2, \omega_2)$, and $(\mathbf{k}_3, \omega_3)$ to generate a signal with $\mathbf{k}_s = \mathbf{k}_1 - \mathbf{k}_2 + \mathbf{k}_3$; $\omega_s = \omega_1 - \omega_2 + \omega_3$. Both SRS and CRS have developed into powerful analytical and diagnostic tools for vibrational motions [1].

These techniques can be extended to the x-ray regime, where the high-frequency beams create core hole excitations and the low-frequency Raman resonances correspond to valence optical excitations. Spontaneous x-ray Raman scattering (SXRS) has been extensively applied to molecules in the gas phase [2], and to strongly correlated crystals [3]. However, the coherent analogue, CXRS, has not been reported yet, since x-ray nonlinear optics has been made possible only by recent progress in the generation and control of x-ray pulses [4].

In this Letter, we simulate the CXRS signal for a model molecular system and demonstrate its utility as a novel probe for electronic transitions. By tuning the frequencies and wave vectors of the three incoming fields, CXRS provides detailed information on low-frequency optical excitations. Since soft-x-ray ($\sim$10 Å$-$100 Å) wavelength is comparable to a molecular size, the dipole approximation which imposes strict selection rules in optical spectroscopy does not apply, allowing the direct probing of the entire manifold of electronic transitions. Another consequence of the short wavelength is the strong wave vector dependence of the CXRS signal. By tuning the x-ray frequencies across the core excitation of various atoms, it becomes possible to investigate precisely the nonlocal nature of the valence electronic excitation. CXRS further allows the direct observation of excitation energy transfer between atoms within a molecule. This is a clear advantage over SXRS which takes place at the same atomic site and cannot probe spatial coherence over different atoms. In addition, CXRS can be effectively used to characterize the core-excited states. The wave vector dependence is caused by x-ray transitions at different atomic sites, and carries information on the distance between atoms responsible for different x-ray absorption peaks.

A single-body picture of the CXRS process is depicted in Fig. 1(a) where the open and hatched blocks represent unoccupied conduction and unoccupied valence states, respectively, and two deep core levels at different atomic sites are also shown. The two beams with frequencies ω_1 and ω_2 are resonant with the core excitation of a particular atom (site a), whereas the third beam with frequency ω_3 and the signal ω_s x-ray beam are resonant with the core excitation of another atom (site b).

The interaction with the $\mathbf{k}_1$ and $\mathbf{k}_2$ beams creates a polarization associated with the valence exciton at site a (pair creation of the valence hole and the conduction electron). This polarization is then probed at site b by the combination of the $\mathbf{k}_3$ beam and the signal beam $\mathbf{k}_s$. Only when the valence exciton state is delocalized over these two sites, we have a significant wave vector dependent CXRS signal.

We have simulated CXRS of a one-dimensional molecular chain with $N = 8$ atoms, each having three (core, occupied valence, and unoccupied conduction) orbitals. We include the transfer of the conduction electron (t_c) and valence hole (t_v), but neglect core hole transfer. On-site attractive Coulomb interactions between a core hole and a conduction electron (core-exciton effect) (U_{ac}), between the valence hole and a conduction electron (valence-exciton effect) (U_{vc}), and the on-site repulsive Coulomb interaction between conduction electrons (U_{cc}) are taken into account, in addition to the Coulomb repulsion between core holes (U_{aa}). Since states with two valence holes do not contribute to the present $\chi^{(3)}$ process, we did not include the Coulomb repulsion between valence holes. The interaction and energy parameters for all sites are given in Fig. 1(b), where the orbitals for the

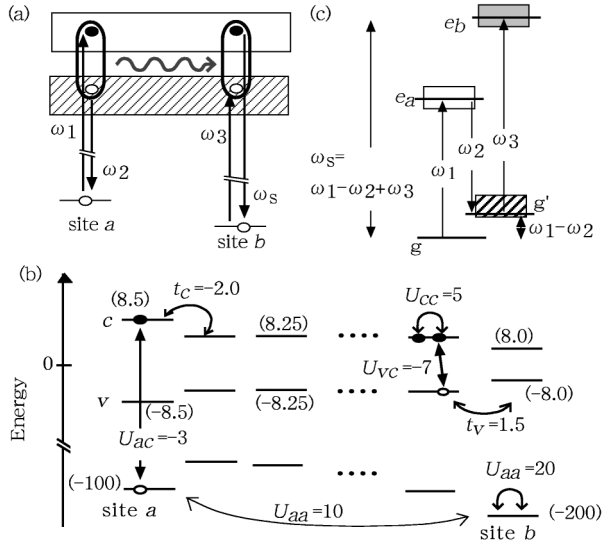

FIG. 1. (a) One-body picture of CXRS. The open and hatched blocks are unoccupied conduction and unoccupied valence states, respectively. (b) One-dimensional molecular chain model system. The strengths of the interactions are written (in eV) and the site energies are given in parentheses. (c) Level scheme for CXRS.

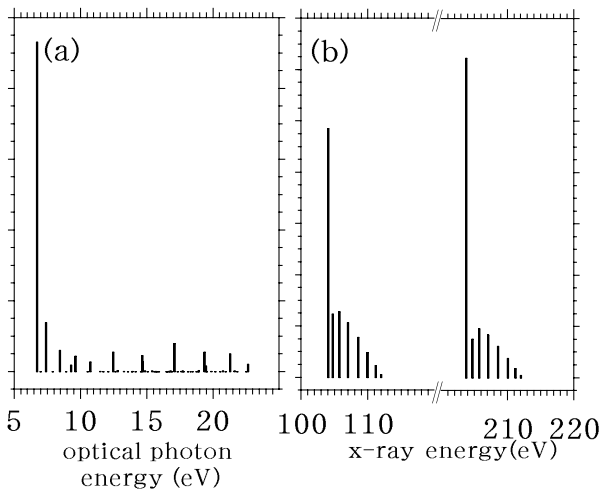

FIG. 2. The calculated optical absorption (a) and x-ray absorption spectra (b).

intermediate sites are not drawn for clarity. We assume that the core-excited state energies of site a (e_a) and site b (e_b) are well separated. The energy level scheme is shown in Fig. 1(c), where the core-excited state energy of site a, site b, and optical excited states are depicted by open, shaded, and hatched boxes, respectively. We have neglected the charge redistribution effect induced by core excitation. The reason is that, in the present model, the core electron is resonantly excited to a strongly bound core exciton state where the charge neutrality around the excited atom is maintained. Valence relaxation becomes important only when the core electron is excited to a high energy continuum, the molecule is ionized, and the core hole screens the Coulomb potential, strongly affecting the electronic levels by creating shakeup states [5].

The eigenstates of the model Hamiltonian were computed by direct diagonalization using the basis set of the single-core-excited, double-core-excited, and optically excited states. The coupling of the molecule with a resonant radiation x-ray field $\hat{A}(\mathbf{r}, t)$ is $\hat{H}_{int} = -\sum_{n=1}^{N} \hat{j}_n \hat{A}(\mathbf{R}_n, t)$, where $\hat{j}_n$ is the atomic current density operator [6] at site n ($\mathbf{R}_n$). We retain only on-site atomic radiative transitions and neglect cross transitions between weakly overlapping orbitals at different sites. The optical absorption spectrum is shown in Fig. 2(a). Since the Coulomb attraction ($U_{vc} = -7$ eV) between a valence hole and a conduction electron is large, the strongly bound valence exciton states lie below the loosely bound exciton states: The model shows Frenkel(Wannier)-type exciton states below (above) $\sim$10 eV. The optical absorption spectrum is concentrated on the lowest exciton $\mathbf{k} = \mathbf{0}$ state at 6.7 eV. In addition, we see many weak transitions between 6.98 to 22.7 eV. The x-ray absorption spectra are shown in Fig. 2(b), where the absorption lines from 104.05 to 112 eV and those from 203.77 to 212 eV are attributed to the core excitation at site a and site b, respectively, with strong origins at 104.05 and 203.77 eV.

We consider a three beam CXRS where ω_1 and $\omega_s = \omega_1 - \omega_2 + \omega_3$ are resonant with the core-excited states and $\omega_1 - \omega_2$ is tuned across the optical excitation energy. The third order nonlinear susceptibility relevant for CXRS is $\chi^{(3)}(-\mathbf{k}_s, -\omega_s; \mathbf{k}_1, \omega_1, -\mathbf{k}_2, -\omega_2, \mathbf{k}_3, \omega_3)$. While homodyne detection gives $|\chi^{(3)}|^2$, heterodyne detection allows to probe $\chi^{(3)}$ itself: both $\mathrm{Re}[\chi^{(3)}]$ and $\mathrm{Im}[\chi^{(3)}]$.

The general formal expressions for the frequency and wave vector dependent third order susceptibility $\chi^{(3)}$ for our model system, and the seven Liouville space pathways showing the various contributions to x-ray four-wave mixing under the rotating wave approximation, are given in Appendices A and B of Ref. [7]. Because of the fast Auger decay, the lifetime of the core-excited states ($<$10 fs) is much shorter than the optically excited states (ps to ns). As a result, the dominant contributions to CXRS come from the R_{IV} pathway [7] which include only the single-core-excited states and the optically excited states. We then have

$$\chi^{(3)} \approx R_{IV} = \sum_{g'} \alpha_{gg'}(\omega_1, \omega_s) \frac{1}{\omega_1 - \omega_2 - \omega_{g'g} + i\Gamma_{g'g}}, \quad (1)$$

where

$$\alpha_{gg'}(\omega_1, \omega_s) = \sum_{m,n} \sum_{e_m} \sum_{e_n} \exp[i\mathbf{q} \cdot (\mathbf{R}_n - \mathbf{R}_m)] \cdot \frac{j_{g,e_m} j_{e_m,g'}}{\omega_s - \omega_{e_m g} + i\Gamma_{e_m g}} \times \frac{j_{g',e_n} j_{e_n,g}}{\omega_1 - \omega_{e_n g} + i\Gamma_{e_n g}}, \quad (2)$$

with m and n running over the core sites. Note that $\alpha_{gg'}$

depends on ω_3 as well as ω_1 and ω_2 through the relation $\omega_s = \omega_1 + \omega_3 - \omega_2$. e_n (e_m) denotes the eigenstates of the single-core-excited state for site n (m), g' denotes the optically excited state, and $\mathbf{q} \equiv \mathbf{k}_1 - \mathbf{k}_2$ is the grating wave vector. In Eq. (2) $\omega_{\xi\eta} \equiv (E_\xi - E_\eta)/\hbar$ and $\Gamma_{\xi\eta}$ are the frequency and the dephasing rate corresponding to the ξ to η transition [1,6]: $\Gamma_{e_m g} = 64$ meV and $\Gamma_{g'g} = 1$ meV. It should be emphasized that, as seen from Eqs. (1) and (2), the linewidth of the Raman resonances is determined by the valence-exciton dephasing rates $\Gamma_{g'g}$. The much larger core hole linewidth Γ_{eg} corresponding to the Auger decay merely affects the magnitude of the signal, but not the linewidth. The technique therefore has a high spectral resolution. Furthermore, ionization induced by Auger decay will not interfere with the signal since it is possible to selectively excite the neutral molecule by tuning the x-ray frequency to the core resonance of the neutral molecule, as is commonly done in photoemission spectroscopy [2].

It should be noted that CXRS depends only on the grating wave vector $\mathbf{q}$, since the wave vector dependence at site n is $\exp[i\mathbf{q} \cdot \mathbf{R}_n]$ and at site m is $\exp[-i(\mathbf{k}_s - \mathbf{k}_3) \cdot \mathbf{R}_m]$, but due to phase matching $\mathbf{q} = \mathbf{k}_s - \mathbf{k}_3$. When ω_1 and ω_s are resonant with core excitations at different sites ($m = a$ and $n = b$), the phase of the CXRS signal varies periodically with $|\mathbf{q}| = 2\pi/|\mathbf{R}_a - \mathbf{R}_b|$. By tuning the three frequencies, we can select specific contributions to CXRS.

We first tune all three frequencies to be near resonant with the core excitation at site a. The term with $m = n = a$ in Eq. (2) dominates the CXRS when ω_1 and ω_s are near resonant with the core excitation energy of site a. The calculated homodyne CXRS signal ($|\alpha_{gg'}|^2$) is shown by log scale in Fig. 3(a) vs $\omega_1 - \omega_2$, where ω_1 is fixed at 104.05 eV (core-exciton peak at site a), and ω_3 is linearly scanned with ω_2 so that ω_s is held at 103 eV just below the core-exciton peak. The signal has an intense sharp line at 9.63 eV attributed to the strongly localized Frenkel exciton state at site a, while the peaks corresponding to the other valence exciton states are much weaker. The CXRS spectrum is quite different from the SXRS signal shown in Fig. 3(b), where the incident x-ray frequency is tuned to 104.05 eV. The Frenkel exciton peaks other than the 9.63 eV peak and the Wannier exciton peaks between 10.5 to 22.7 eV are stronger than in CXRS. The weaker peaks are relatively stronger in SXRS because the homodyne CXRS signal intensity is given by $|\chi^{(3)}|^2$. The weak peaks can be better seen in heterodyne detection which probes $\chi^{(3)}$ itself.

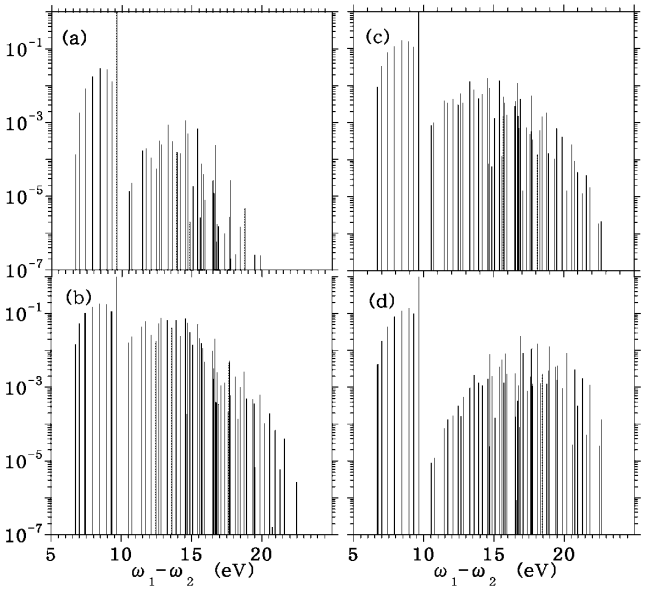

FIG. 3. (a) CXRS, (b) SXRS, (c) the ratio of CXRS to SXRS, and (d) the local component of the optical absorption $|j_{g,g'}(a)|^2$ (log scale).

When ω_1 is resonant with one of the core-exciton states while ω_s is fixed at an off-resonant frequency, which is the case in Fig. 3(a), we can use a sum rule for the core-excited state in Eq. (2) to obtain

$$\alpha_{gg'}(\omega_1, \omega_s) \approx j_{g,g'}(n) \sum_{e_n} \frac{j_{g',e_n} j_{e_n,g}}{\omega_1 - (\omega_{e_n} - \omega_g) + i\Gamma_{e_n,g}}. \tag{3}$$

The CXRS signal is then given by a simple product of $|j_{g,g'}(n)|^2$, and the scattering amplitude of the SXRS. Obviously $|j_{g,g'}(n)|^2 \equiv |\langle g'|\hat{j}_n|g\rangle|^2$ ($n = a, b$) represents the local contribution to the $|g\rangle$ to $|g'\rangle$ optical excitation. This is confirmed in Fig. 3(c), which shows that the ratio of CXRS to SXRS closely resembles $|j_{g,g'}(a)|^2$ shown in Fig. 3(d). We can therefore directly obtain the local contribution to the optical excitation from the ratio of CXRS and SXRS.

We next consider the case when ω_1 and ω_s are resonant with different sites e_a and e_b, respectively, as depicted in Fig. 1. In Fig. 4, we show the real part of $\alpha_{gg'}$ for various values of $\mathbf{q}$ when $\omega_1 = 104.05$ eV and $\omega_s = 203.77$ eV are resonant with the core-exciton peak of site a and site b, respectively. Since ω_1 and ω_s are resonant with the strongly localized core-exciton states, the peaks corresponding to the Frenkel exciton states have a strong intensity at 6.7 to 9.63 eV and a strong $\mathbf{q}$ dependence compared to the Wannier exciton states above 10.5 eV. In this case, we have $\alpha_{gg'}(\omega_1, \omega_s) = -\exp[i\mathbf{q} \cdot (\mathbf{R}_a - \mathbf{R}_b)] j_{g,e_b} j_{e_b,g'} j_{g',e_a} j_{e_a,g} / \Gamma_{e_b g} \Gamma_{e_b g}$. Since the e_a and e_b core-exciton states are localized at the corresponding sites, we have $\alpha_{gg'} \propto \exp[i\mathbf{q} \cdot (\mathbf{R}_a - \mathbf{R}_b)] j_{g,g'}(b) j_{g',g}(a)$. The heterodyne CXRS thus acquires a $\mathbf{q}$-dependent phase (which is missed by homodyne detection). In contrast, SXRS is a local process where all transitions take place at the same site and show no $\mathbf{q}$ dependence.

Figure 5 depicts the $\mathbf{q}$ dependence of the various exciton peaks of Fig. 4. Unlike the lowest (6.7 eV) and the highest energy (9.63 eV) exciton states, the 7 to 9.3 eV peaks show a strong $\mathbf{q}$ dependence. This is because, while the exciton states at 9.63 eV are strongly localized at site a, the 7 to 9.3 eV states are delocalized over sites a and

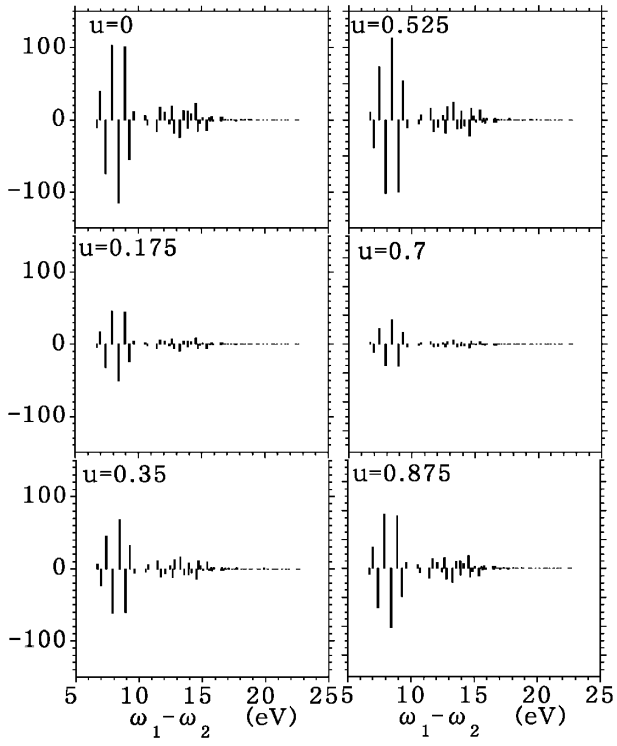

FIG. 4. Wave vector dependence of CXRS when $\omega_1 = 104.05$ eV and $\omega_s = 203.77$ eV. The grating wave vectors are $q = 2\pi u/|\mathbf{R}_a - \mathbf{R}_b|$, for various values of u as indicated.

b. As is well known in exciton theory, if the valence exciton is delocalized, the exciton band has a large dispersion: That is, the exciton energy strongly depends on the wave vector. The weak $\mathbf{q}$ dependence of the 6.7 eV state indicates that it includes a small component of $j_{gg'}(a)$ and $j_{gg'}(b)$: The 6.7 eV state is described as the sum over the intermediate sites between site a and site b. Since all peaks change periodically with $|\mathbf{q}| = 2\pi/|\mathbf{R}_a - \mathbf{R}_b|$, the heterodyne CXRS may be used to trace the origin of the x-ray absorption lines: If the core excitation energies of different sites are nearly degenerate, the x-ray absorption lines of sites a and b are not well resolved. By tuning ω_1 and ω_s to different absorption peaks and observing the $\mathbf{q}$ dependence, we can trace the sites where the various absorption peaks originate from, and their separation. When the system contains several sites with nearly degenerate core-exciton energies, the $\mathbf{q}$ dependence of the signal through Eq. (2) should carry a clear signature of excitation transport. In this case, the $\mathbf{q}$ dependence is not merely through the phase. Optical transient grating experiments of excitations are commonly used to observe long wavelength diffusion [8]. X-ray gratings such as in CXRS should allow one to probe the dynamics of excitations on a much finer length scale. The wave vector dependence in Figs. 4 and 5 was calculated for an oriented sample. Averaging over random angular distribution of molecules in Eq. (2) will turn the exponential factor into $J_0(q|\mathbf{R}_a - \mathbf{R}_b|)$, where $J_0(x)$ is the zeroth order Bessel function. This will affect the relative intensities of the various CXRS peaks, but their wave vector dependence should still be clearly visible.

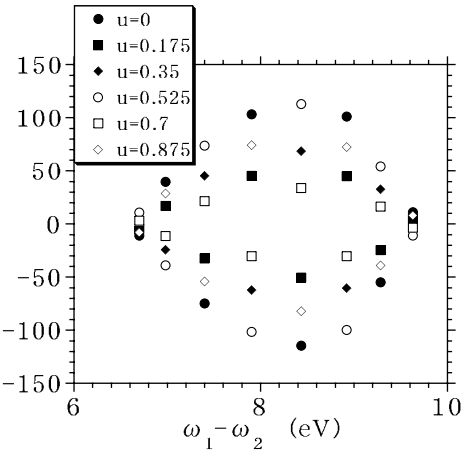

FIG. 5. Wave vector dependence of CXRS for the exciton peaks of Fig. 4.

Using the C $1s \rightarrow 2p$ atomic dipole transitions in polydiacetylene, we have estimated the magnitude of $\chi^{(3)}$ and found it to be about 3.5×10^{-12} esu under fully resonant conditions. Although this is 2 to 3 orders of magnitude smaller than $\chi^{(3)}$ in the optical region [9], recent progress in the generation of intense femtosecond spatially coherent x-ray pulses by high harmonic generation should make these measurements feasible.

This work was partly supported by a Grant-in-Aid for Scientific Research from the Ministry of Education, Science, Sports, and Culture in Japan. The support of the National Science Foundation Grant No. CHE-0132571 is gratefully acknowledged.

[1] S. Mukamel, *Principles of Nonlinear Optical Spectroscopy* (Oxford University, New York, 1995).
[2] F. Gel'mukhanov and H. Ågren, Phys. Rep. **312**, 87 (1999).
[3] A. Kotani and S. Shin, Rev. Mod. Phys. **73**, 203 (2001).
[4] M. Drescher *et al.,* Science **291**, 1923 (2001); R. W. Schoenlein *et al.,* Science **287**, 2237 (2000).
[5] M. S. Deleuze and L. S. Cederbaum, Adv. Quantum Chem. **35**, 77 (1999).
[6] S. Tanaka *et al.,* Phys. Rev. A **63**, 63405 (2001).
[7] S. Tanaka and Shaul Mukamel, J. Chem. Phys. **116**, 1877 (2002).
[8] T. S. Rose, R. Righini, and M. D. Fayer, Chem. Phys. Lett. **106**, 13 (1984).
[9] P. A. Gass *et al.,* J. Chem. Phys. **100**, 88 (1994).